Multi-Gateway LoRaWAN Throughput Modeling in Direct-to-Satellite IoT Constellations

Santiago M Henn, Juan Andrés A Fraire, Nicola Accettura, Sandra Céspedes, Holger Hermanns

Multi-Gateway LoRaWAN Throughput Modeling in Direct-to-Satellite IoT Constellations

Santiago M. Henn*, Juan A. Fraire*†‡, Nicola Accettura§, Sandra Céspedes¶, Holger Hermanns‡
*CONICET - Universidad Nacional de Córdoba, Argentina
†Inria, INSA Lyon, CITI, UR3720, 69621 Villeurbanne, France
‡Saarland University, Saarland Informatics Campus, Saarbrücken, Germany
§LAAS-CNRS, Université de Toulouse, CNRS, Toulouse, France
¶CSSE Department, Concordia University, Montreal, QC, Canada

***Abstract*—The emerging paradigm of Direct-to-Satellite Internet of Things (DtS-IoT) heralds a new era of global IoT connectivity unlocked by gateways in Low-Earth Orbit (LEO). Among the spectrum of technologies for achieving DtS-IoT, LoRaWAN, which relies on duty-cycled ALOHA channel access over unlicensed bands, emerges as a promising candidate. LoRaWAN's broad adoption in terrestrial IoT applications paves the way for a seamless Space-Terrestrial IoT integration. LoRaWAN distinctively allows multiple gateways to receive uplink packets simultaneously, an appealing feature for proliferated DtS-IoT constellations leveraging multiple satellites. However, existing theoretical throughput models for static multi-gateway LoRaWAN systems have not been evaluated in the more complex and dynamic satellite context. Our study addresses this gap by adapting, extending, and fine-tuning throughput models for the multi-gateway LEO DtS-IoT scenario. This approach will enable the rapid analysis of various LoRaWAN constellations to optimize their performance, addressing a critical need in current DtS-IoT mission design and operations. Additionally, we validate the proposed modeling with a comprehensive and realistic simulation campaign. Differences between the model predictions and simulation results remain below 5%. Results show that the proposed modeling is accurate and insightful, offering valuable projections into the performance of forthcoming LoRaWAN DtS-IoT constellations.**

***Index Terms*—Throughput models, Satellite Constellations, Direct-to-Satellite IoT, Constellation Coverage**

I. Introduction

The Internet of Things (IoT) ecosystem is vast. It involves using cellular networks, narrow-band devices, and short- and medium-range sensors, all operating at high and low data speeds [1]. In this context, low-power wide-area networks (LPWANs) are a type of IoT capable of connecting devices where only small amounts of information need to be transmitted over long distances (100km, at $<$ 50Kbps) [2]. LPWAN applications include agriculture, environmental monitoring, and emergency management, among others [3].

These applications require communication services in vast regions, especially those lacking terrestrial infrastructure, and in such cases, satellite communications become a natural and even indispensable resource [4]. In this regard, it is logical to resort to geostationary satellites (GEO) as a potential solution. However, in comparison, satellites in low Earth orbit, or LEOs as they are commonly referred to in the industry jargon, offer more lenient link requirements and delay [5]. LEO satellites orbit at altitudes between 300 km and 1000 km, which means their orbital speed is around 7 km/s. Consequently, the visibility intervals with a ground station, when possible, are on the order of 10 minutes [6].

One of the various strategies for providing global IoT services is using satellites as a backup link to transport information from gateways on Earth, thus operating as an indirect relay of the data generated by End Devices (EDs) [7]. This indirect approach, called Indirect IoT, is appealing in densely populated and highly accessible urban areas, where a massive concentration of EDs encourages the deployment of dedicated terrestrial IoT gateways. This setup can leverage LEO or GEO satellites to relay data to and from the EDs. On the other hand, some applications in less accessible regions (e.g., agricultural production matrix, oceans, mountain chains, poles) may not justify or even hinder the deployment of support infrastructure on Earth. A more attractive but challenging architecture in these latter scenarios would involve directly linking one or many EDs with gateways aboard satellites. This scheme, called Direct-to-Satellite IoT (DtS-IoT), has received increasing attention from industry (startups such as Lacuna Space, Sateliot, among others) and academia [8], [9]. Additionally, unlike the indirect approach, DtS-IoT motivates the study and possible enhancements of standard LPWAN protocols to address the challenges of space-ground link [10], [11].

Some LPWAN technologies operate in portions of the unlicensed radio spectrum, reducing implementation costs and improving accessibility. The LPWAN architectures are hierarchical, with gateways acting as data collectors for EDs [7]. An established LPWAN technology is LoRaWAN [12], which in its physical layer uses modulation techniques based on CSS (Chirp Spread Spectrum) [13], [14], thus achieving low data rate but long-range communication and low power consumption. NB-IoT is another LPWAN technology that shows promise in satellite applications. However, we analyze LoRaWAN for satellite constellations due to its superior power efficiency, lower deployment costs, use of unlicensed spectrum, and simpler network architecture [15]. Despite this, with its higher data rates and growing adoption, NB-IoT presents significant potential and should be addressed in future works to explore its viability and advantages in satellite-based IoT networks. In LoRaWAN, channel access is based on the

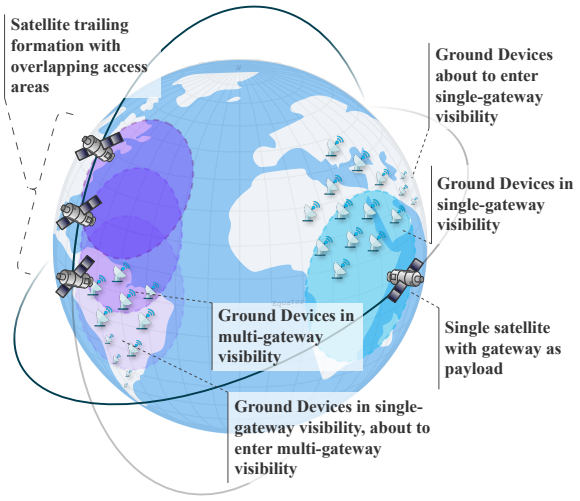

Fig. 1: Visualization of Single-Gateway and Multi-Gateway Configurations: Comparison between Monolithic Satellites and Satellite Constellations or Formations.

pure ALOHA protocol, and network devices do not have an admission control policy. The LoRaWAN standard imposes a limitation or duty cycle on the traffic generated by EDs to improve channel performance over the unlicensed band. After each transmission, an ED must remain silent for a certain period determined according to the region [16].

While there are analytical models to predict performance in static LoRaWAN deployments, single and multi-gateway [17], these have not been studied for their potential application in satellite IoT constellations. Single-satellite studies have only focused on device synchronization aspects [18]. Performance analysis of EDs, optimal transmission rates, optimal node density, etc., for a given duty cycle, can help national standardization bodies choose appropriate limitations for satellite missions, using this link to define optimal mission requirements.

This work proposes a novel analysis methodology for LoRaWAN-based DtS-IoT that introduces analytical models for network throughput, specifically in a multi-gateway satellite mission context. In pursuit of this objective, established models from static networks are integrated with state-of-the-art astrodynamics tools, constellation coverage computing methods, and discrete simulations to validate the theoretical models and explore their viability in guiding the design and operation of space missions. This investigation encompasses scenarios involving single-gateway and multi-gateway configurations, corresponding to monolithic satellites and constellations or formations, respectively, as illustrated in Figure 1. Our model tackles the complexities that the so-called "constellation-to-ground coverage problem" introduces into constellation-based networks [19]–[21] which refers to the challenges of computing the coverage regions of a constellation, either instantaneously or over a simulation period [22]. This is achieved by employing techniques to efficiently evaluate the intersections and temporal drift of a constellation's access regions and their relationship with EDs.

Regarding the organization of the work, Section II analyzes related works relevant to the present research. Section III presents the models used, characterized in three defined regions. Section IV presents the simulation methodology that will serve as the basis for the model comparison. Section V presents a case study along with its results regarding the fit between analytical predictions and simulations. Section VI concludes the work and presents some future developments.

II. Background

The space industry has utilized and continues to use low-power, low-data-rate data transfer technologies. One of the most concrete examples is the ARGOS system [23], which has been operating since 1978 and aims to collect environmental information in locations without local coverage directly to the satellite. Another example are Data Collection Systems (DCS), which collect data from devices often deployed in remote and isolated locations [24]. However, these technologies have not been prominently addressed under IoT, whose terminology is relatively new. Although these systems are currently operational, they are not prepared to integrate with terrestrial LPWAN technologies [25], currently implemented by LoRaWAN and NB-IoT.

A. LoRa and LoRaWAN

Among the LPWAN technologies, LoRa (Long Range) implements a modulation technique based on CSS signals [26], particularly attractive for satellite links as it provides very low energy consumption and a large link margin [2]. LoRa modulation can operate in frequency bands that do not require licensing, such as the Industrial, Scientific, and Medical (ISM) bands, which is advantageous in terms of regulations that would otherwise require complex approval procedures dependent on the region [27]. However, ISM bands are not allocated for space services, so they still require appropriate licenses and coordination with the International Telecommunication Union (ITU) [28].

A significant milestone in DtS-IoT was the deployment of LacunaSat-1, the first LoRaWAN nano-satellite by Lacuna in 2019, which validated the DtS-IoT model, as reflected in related experiments [29]. Additionally, scientific works including long-range evaluations [30], modulation improvements for LEO links [31], Doppler effect evaluations [32], and adaptations for space links based on LoRa [33], converge on the feasibility of these communications.

On the LoRa modulation, LoRaWAN is the specification responsible for the medium access layer service, enabling data management over bidirectional and asynchronous links [34]. LoRaWAN operates on a distributed topology where gateways function as data concentrators, enabling EDs to connect to a centralized network server on the Internet. This topology can be visualized as a "star of stars" or a directed acyclic graph [35]. The specification supports data rates ranging from 0.3 kbps to 50 kbps through three service classes or device classes explained below:

1) Class A is the most basic mode yet energy-efficient, where a ED turns on the radio only to perform a transmission and then goes into a receive window for two time slots before turning it off again.
2) Class B devices add receive windows at fixed intervals to synchronize with the gateway via beacon messages at the cost of slightly higher consumption than Class A.
3) Class C devices, assumed to have an external power source, operate in continuous receive mode, generating the highest consumption.

B. Previous Works on Throughput Models

To model the network's throughput, it is first necessary to establish the transmission behavior and strategies of EDs based on the degrees of freedom the protocols allow. The LoRaWAN standard proposes a medium access based on pure ALOHA, although versions with slots or frames that improve performance are found in the literature [36]. With this in mind, in [14], the authors address the scalability of LoRaWAN.

Regarding a mathematical model that allows predicting the operation of a LoRaWAN network, there are precedents for the protocol in ACK mode with retransmissions, including performance analysis, in [37] without capture effect and in [38] with capture. In [39], the impact of retransmissions on network lifetime is analyzed, while in [40], a stochastic geometry-based approach is used for scalability analysis for a single gateway, and in [41] for multiple gateways. However, these models do not consider limitations in the duty cycle, which is necessary to comply with the regulations in each region.

In [17], Accettura and Prabhu examined throughput in static multi-gateway LoRaWAN networks with and without duty cycle limitations, deriving formulas for various scenarios, such as regularly tiled multi-gateway networks and applications like radio localization.

Authors in [42] introduced FLoRaSat, an event-driven open-source end-to-end simulation tool designed to address the challenges of Direct-to-Satellite Internet of Things (DtS-IoT) networks, which utilize LEO satellites as gateways for IoT devices in remote areas that can operate using LoRaWAN protocols. While this tool addresses throughput and performance evaluation in DtS-IoT networks, it relies solely on numerical results generated from simulated traffic. Chasserat et al. introduce LoRaSync in [43], an energy-efficient synchronization scheme for LoRaWAN networks, addressing scalability issues caused by frame collisions. While they effectively tackle the issue of throughput maximization in single-gateway deployments, they do not consider multi-gateway or satellite-based architectures. More recently, Tondo et al. introduced two novel multiple-access scheduling strategies for DtS-IoT networks, addressing the challenges of energy and spectral efficiency [44] on satellite-based single-gateway LoRaWAN systems, improving throughput through synchronization and performing validations solely through simulations. The previous work has partially addressed throughput modeling in single and multi-gateway LoRaWAN systems, leveraging simulations for satellite-based and ground-based schemes.

To date, we have been unable to identify any existing research that addresses the task of expanding analytical throughput models for single and multi-gateway satellite-based LoRaWAN networks while assessing their accuracy and validating their practical applicability. The existing research in this area shows significant room for improvement. By incorporating analytical and semi-analytical models, it would be possible to enhance result validation and broaden the range of scenarios that can be analyzed.

III. Analytical model

The characterization of DtS scenarios relies on three pivotal components: the satellite orbit(s) serving as the platform for the gateway, the Earth model coupled with the deployment rules for EDs, and lastly, the specifications of the communication protocol and how network traffic is generated.

A. Access Intervals Prediction and Constellation Coverage

Orbital propagation represents a significant portion of the computational time needed for satellite coverage analysis. For single-gateway deployments, this involves predicting the satellite's position over time, considering all necessary orbital perturbations. Access intervals for a given position on Earth are determined by obtaining the time instant when the satellite starts to meet the necessary conditions to establish radio communication with an ED in that position. Obtaining the precise instant requires accurate orbital propagation over time, and hence, an analytical formulation of the orbit allows for sub-sampling and convergence procedures. High-precision orbital propagators rely on computationally costly integration algorithms. Pure analytical procedures based on unperturbed models, although orders of magnitude faster than high-precision ones, imply errors as the propagation time increases [6]. An intermediate model, known as SGP4, for *Simplified General Perturbations model 4*, proposed by David Vallado [45], [46], offers a semi-analytical propagator with good speed and accuracy performance. This model calculates the orbital state vectors of satellites relative to the Earth-centered inertial coordinate system, incorporating a simplified atmospheric friction model and secular and periodic orbital perturbations caused by the Earth's geometry, achieving an error on the order of ~ 1 km that grows at a rate of $\sim 1-3$ km/day.

To address the challenges posed by the constellation-to-ground coverage problem, we utilize polygon-based algorithms [21] that leverage an implementation in Orekit's (Orbital Extrapolation Kit) distribution of SGP4-based tools [47]. These algorithms are built upon the Martinez-Rueda Algorithm [48], which extends the plane sweep technique [49], and utilize the analytical framework developed by Nugnes et al. [50], [51]. This method facilitates rapid identification of regions with a minimum coverage of N satellites at any given time while allowing for the computation of the union and intersection of different combinations of these regions. This approach surpasses traditional and other state-of-the-art methods, which often require more computational resources and overlook critical aspects of the constellation-to-ground topology, such as Earth's oblateness, ground elevation thresholds, and considerations near the poles. Notably, this method

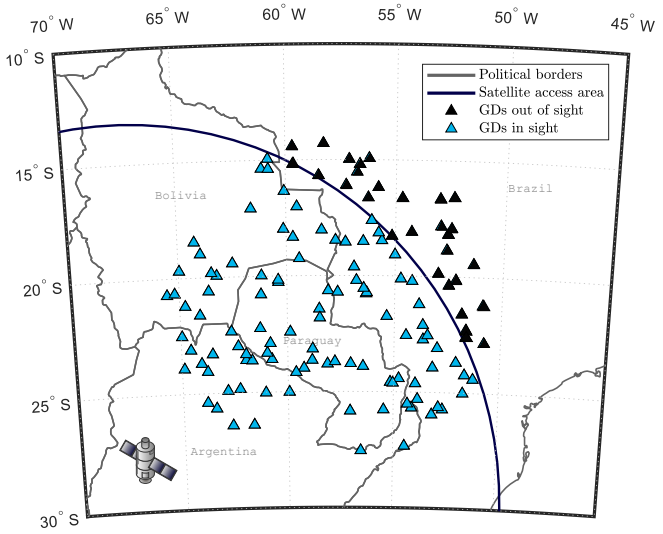

Fig. 2: Example of 130 devices deployed according to a Poisson process in a circular area centered at coordinates $-21°, -58°$ latitude and longitude, respectively.

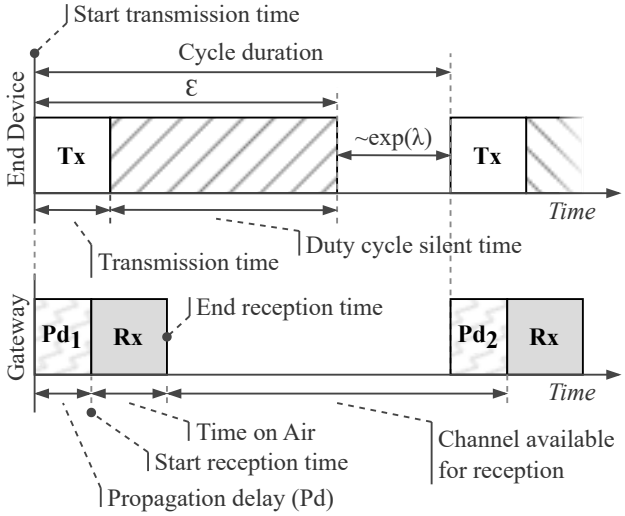

Fig. 3: The evolution of the End-Device state and the life-cycle of transmission and reception schemas.

remains versatile, as it can adapt to any orbital propagator and remains independent of net-point granularity, a fundamental parameter in finite-elements-based (often called net or grid-point) approaches [52]–[57].

In this work, the Earth is modeled using the WGS84[1] system. We define our Ground Device Deployment Regions as polygons drawn over the Earth's surface. We adopt circular deployments centered at a specific geographical coordinate to simplify our analysis. EDs are considered to be randomly deployed within these circular regions, following a Poisson process to ensure uniform distribution, as depicted in Figure 2. During simulations, EDs are deployed, and their positions are computed in Earth-Centered Inertial (ECI) coordinates. Additionally, access intervals to each satellite are determined for the duration of the simulation analysis period.

B. Traffic Generation and throughput estimation in single-gateway deployments

We adopt a traffic generation method that follows a Poisson process. Our model draws inspiration from a static model developed for LoRaWAN, catering to single and multiple gateway deployments [17]. We focus on the uplink traffic of LoRaWAN networks and assume that all transmitted frames are the same size. This results in a specific time-on-air value for all transmissions. We use such a value as unit time to normalize all the variables hereafter defined. For instance, the time between 2 consecutive transmissions is assumed to follow an exponential distribution with an average data generation rate of λ frames per unit time. Hence, the number N_{pkt} of frames generated into x units of time is a random variable modeled as a Poisson distribution with an expected number of occurrences λ per unit of time:

$$\mathbb{P}\left(N_{pkt}(x) = k\right) = e^{-\lambda x}\frac{(\lambda x)^k}{k!}. \tag{1}$$

When a duty cycle limitation applies, an ED can transmit on average 1 frame every ε units of time. The LoRaWAN specification [12] enforces the strictest duty-cycle policy by forcing an ED to stay silent for $\varepsilon - 1$ units of time after having transmitted a frame (see Fig. 3). As in [17], we assume that EDs discard (and do not cache) frames generated during an ongoing transmission or the following enforced silence time. Defining a cycle as the interval between 2 consecutive frame transmissions, it is easy to realize that the effective transmission rate g of LoRaWAN EDs is

$$g = \frac{\lambda}{1 + \lambda\varepsilon}. \tag{2}$$

Furthermore, we consider the EDs deployed under the coverage region Ω centered on a gateway, and whose area is expressed as $\mathcal{A}(\Omega)$. More specifically, EDs are placed over the Earth according to a Poisson Point Process with an average density of μ per unit area. In such a way, the average number of EDs over Ω is $\mu\mathcal{A}(\Omega)$. In [17], it is shown that the throughput value on this region is equal to

$$g\mu\mathcal{A}(\Omega) \cdot e^{-\frac{2}{n}g\mu\mathcal{A}(\Omega)} \tag{3}$$

where n is the number of available channels.

It is worth extending the previous notation to introduce the case of a multi-gateway environment smoothly. Indeed, we introduce the throughput related to any sub-region $\Theta \subseteq \Omega$, as

$$\mathcal{S}_\Omega(\Theta) = g\mu\mathcal{A}(\Theta) \cdot e^{-\frac{2}{n}g\mu\mathcal{A}(\Omega)}. \tag{4}$$

In such a formula, the final throughput is computed as the product of the overall offered traffic $g\mu\mathcal{A}(\Theta)$ from the EDs in the sub-region Θ, and the probability that none of the other EDs deployed on the coverage region Ω do not interfere.

[1]The WGS84 system defines the Earth's shape as an oblate spheroid with a semi-major axis of 6378.137 km, a semi-minor axis of 6356.752314 km and a flattening constant f of 1/298.257223563

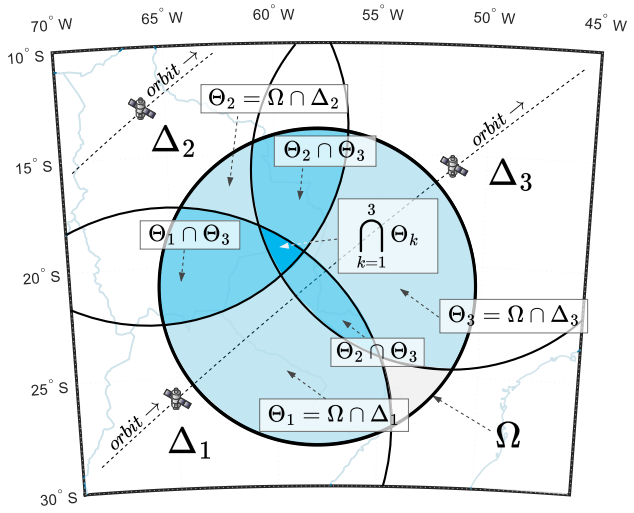

Fig. 4: Deployment area Ω and its intersections $(\Theta_1, \Theta_2, \Theta_3)$ with the satellites' coverage regions Δ_1, Δ_2 and Δ_3.

C. Throughput estimation in multi-gateway deployments

We aim to obtain the average throughput of multi-gateway networks, assuming EDs are randomly distributed according to a Poisson Point Process within a bounded region Ω spanning the Earth's surface and transmit link-layer frames following a Poisson process, as in the single-gateway case. In doing that, we adopt a model that works for an infinite deployment of EDs according to a Poisson Point Process on the Euclidean plane [17] and adapt it to describe the throughput over a bounded region and leverage polygon-based algorithms [21] designed to compute intersections on a Non-Euclidean plane, i.e., the Earth's surface. Considering this model's adaptability to our intended scenarios, we hypothesize that it can effectively accommodate the unique characteristics of multi-gateway deployments over LEO constellations.

Herein, the average throughput is computed as the rate of successful receptions by at least 1 gateway, given that EDs can fall under the coverage range of more than 1 LoRaWAN-enabled LEO satellite. On this regard, by naming as Δ_i the coverage area of the i-th gateway, it must be noticed that EDs positioned within the intersection of multiple Δ_i can communicate with all related gateways. However, interference may occur selectively only on a specific gateway i due to other frame transmissions from EDs placed in the coverage of i but outside the coverage of another gateway j in the considered gateways. For understanding, we refer to the example scenario pictured in Figure 4 to shed some light on the system model. There are 3 gateway-enabled satellites and, as a consequence a set of 3 coverage areas, i.e., $\{\Delta_1, \Delta_2, \Delta_3\}$. Each of these coverage areas intersects the deployment region Ω, thus defining 3 sub-regions $\{\Theta_1, \Theta_2, \Theta_3\}$ (i.e., $\Theta_i = \Delta_i \cap \Omega$). Let's assume an ED is placed within the area indicated with $\Theta_1 \cap \Theta_3$. A frame transmitted while the LEO satellite constellation is passing by will be received by the gateways on board the satellites 1 and 3. However, an ED in the $\Theta_3 \setminus \Theta_1$ sub-region starting a concurrent transmission will originate a frame-collision on gateway 3, while a correct reception will be recorded on gateway 1.

In more detail, given the set Γ of sub-regions $\{\Theta_1, \Theta_2, \ldots\}$ of the Earth's surface, and a subset of it $\Gamma^* \subseteq \Gamma$, the transmissions coming from EDs positioned in the intersection among the sub-regions of Γ^*

$$\mathcal{I}_{\Gamma^*} = \bigcap_{\Theta_i \in \Gamma^*} \Theta_i, \tag{5}$$

can be affected by concurrent transmissions coming from all devices placed in the union among the same sub-regions

$$\mathcal{U}_{\Gamma^*} = \bigcup_{\Theta_i \in \Gamma^*} \Theta_i. \tag{6}$$

Using this notation and leveraging Eq. (4), the rate of successful transmissions from EDs placed within the intersection of sub-regions $\in \Gamma^*$ to "all" related LoRaWAN-enabled LEO satellites is determined as:

$$S^{\Gamma^*} = S_{\mathcal{U}_{\Gamma^*}}(\mathcal{I}_{\Gamma^*}) = g\mu\mathcal{A}(\mathcal{I}_{\Gamma^*}) \cdot e^{-\frac{2}{n} g\mu\mathcal{A}(\mathcal{U}_{\Gamma^*})} \tag{7}$$

With a similar reasoning of [17], applying the inclusion-exclusion principle to cope with the contribution given by each subset Γ^* of the whole set of gateways under reach from Ω, we can find that the rate of successful transmissions to "at least 1 gateway" is

$$S^{\Gamma}_{\Omega} = \sum_{\substack{\Gamma^* \subseteq \Gamma \\ \Gamma^* \neq \varnothing}} (-1)^{|\Gamma^*|-1} S^{\Gamma^*}. \tag{8}$$

We can also rewrite Eq. 8 to consider that the set of sub-regions Γ changes over time

$$S_{\Omega}(t) = g\mu \sum_{\substack{\Gamma^* \subseteq \Gamma(t) \\ \Gamma^* \neq \varnothing}} (-1)^{|\Gamma^*|-1} S^{\Gamma^*}, \tag{9}$$

where the size of $\Gamma(t)$ is related to the set of gateways in a LEO constellations that are in the communication scope of the deployment region Ω, while each element of $\Gamma(t)$ is a sub-region $\Theta_i(t)$ associated to a gateway i, whose shape is determined by the intersection at time t between the coverage area Δ_i and Ω. As we aim to characterize scenarios with fluctuating throughput over time, it is crucial to establish a suitable metric. Therefore, we define the average throughput as akin to the mean signal value over the analysis period T, represented by the following equation:

$$\bar{S}_{\Omega} = \frac{1}{T} \int_0^T S_{\Omega}(t)\, dt \tag{10}$$

IV. Simulation Model

Simulations are conducted using a predefined schema termed a *scenario* to validate the model. This scenario covers a specified analysis period between two dates, producing outputs as time series for subsequent analysis.

A. Scenario assets and dynamics

A scenario comprises several key components or *assets*, including:

- Satellite objects, each equipped with a gateway, may collectively form a formation or constellation.
- The Earth, modeled as an oblate spheroid adhering to the WGS84 model, as detailed in Section III-A.
- A device deployment region is a closed polygon delineated by geographic coordinates across the Earth's surface.
- Transmitter objects deployed within the device deployment region.

Simulating a scenario involves evolving each asset over time according to specific rules governing its position and status. Among these assets, only the device deployment region remains static. The main dynamic rules for each component include:

- Satellite trajectories are defined by their orbital elements, and their positions over time are calculated using an orbital propagator. Here, we utilize an SGP4 propagator, as detailed in Section III-A. Additionally, the gateway, serving as the satellite's payload, can either be in the process of receiving a packet or awaiting a transmission.
- The Earth's evolution over time is governed by its four primary movements: Rotation, Revolution, Precession, and Nutation. While Rotation is the most significant for short-spanned LEO-based scenarios, the SGP4 propagator accounts for Earth's precise position to compute orbital perturbations.
- In terms of position, Transmitter objects are considered static in Earth Centered Earth Fixed (ECEF) coordinates but move in inertial coordinates, depending on their position on the Earth and the Earth's movements. Regarding status, a transmitter can be either transmitting or blocked due to Duty Cycle limitations.

The dynamic behavior of the scenario will be characterized by several discrete snapshots, each separated by a timestep ts. Thus, our analysis for a scenario spanning a timespan T will consist of a time series with $N = \frac{T}{ts}$ points. During procedural simulation of the scenario, access intervals between transmitters and satellites are determined using a software-based event detector integrated into Orekit. A time interval aggregation process is then conducted for each access interval to ascertain which satellites are simultaneously within the radioelectric visibility of the transmitter. These results will serve as the input for a second layer of simulations, grouped under a schema we term *Network*.

B. Network

The Network serves as the digital environment where transmissions occur over time. Each deployed transmitter contributes to the overall traffic and updates its status according to the rules defined in Section III-B. During one ToA unit transmission period, a packet is sent, followed by the transmitter blocking itself for $\varepsilon - ToA$ units of time. This packet propagates through open space within a projected

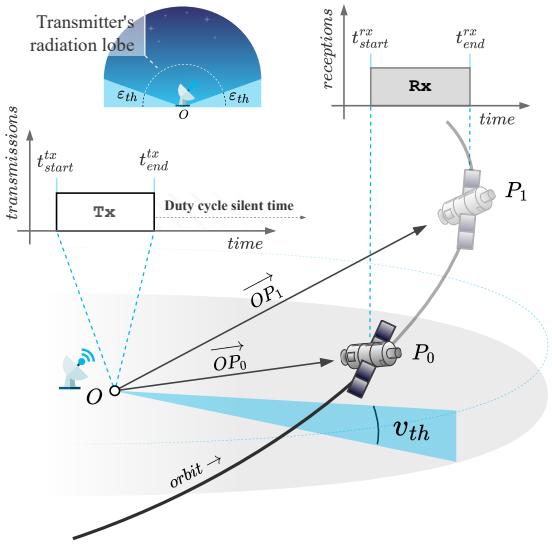

Fig. 5: Illustration depicting the topology of a scenario. Here, a transmitter sends a packet to a gateway, with P_0 and P_1 denoting the satellite's positions at the arrival of the first and last bit of the transmission, respectively.

cone centered on the transmitter's position, based on an elevation threshold v_{th} over the horizon, as shown in Fig. 5. For instance, a satellite and its gateway can receive the transmission if they are above a specific elevation determined by the transmitter's topocentric coordinates (O). If the gateway is in motion relative to the transmitter, the distance between them changes over time, and thus, the transmission reaches the gateway after a computable propagation delay.

1) Traffic Generation: As described on III-B, given a certain mean transmission generation rate λ, transmissions events for a particular transmitter are generated at intervals T_{next} given by:

$$T_{next} = \frac{-ln(1-R)}{\lambda} \tag{11}$$

where R is a pseudo-random number in the $[0, 1]$ interval and λ is the rate in $\frac{events}{second}$. Traffic generation is strategically orchestrated, capitalizing on the memory-less property of the Poisson distribution governing inter-arrival times. This property obviates the need for traffic generation beyond the relative proximity of an access interval with a satellite. To accomplish this, traffic generation initiates at a random time point within an interval that features a probability of 99.9% of containing a transmission, expressed as:

$$T^{-} = \frac{-\ln(1-P)}{\lambda} = \frac{-\ln(0.001)}{\lambda} \tag{12}$$

where T^{-} represents the initiation time, λ denotes the Poisson distribution's rate parameter, and P signifies the probability threshold. If a duty cycle is enforced, the average transmission rate g from Eq. 2 is used instead of λ. Notably, initiating

traffic generation before this interval doesn't influence the outcomes but diminishes performance. This arises because we only need to ensure that device transmitting events are uniformly distributed over time. In theory, traffic generation could commence at a point infinitely distant from the past; however, initiating traffic generation further back only imposes an unnecessary computational burden on the simulator.

2) Signal Propagation and reception dynamics: Transmissions must cover a distance before reaching a gateway, as illustrated in Fig. 5. This process involves determining the satellite's position at the onset and conclusion of packet arrival, factoring in the temporal relationship between the transmitter and the gateway. For a given packet i, the start transmission time $t_{st}(i)$ is computed using the procedures outlined in the previous section. In contrast, $t_{et}(i)$, the end transmission time, extends from $t_{st}(i)$ by the transmission's duration. Let t_{sr} and t_{er} denote the gateway's start and end reception times, respectively. If the transmitter's position is O, and the positions of the satellite upon arrival of the first and last bits of the transmission are P_0 and P_1, respectively, the start reception time (t_{sr}) is calculated as follows:

$$t_{sr} = t_{st} + \frac{\left|\overrightarrow{O, P_0}\right|}{C} \tag{13}$$

and the end reception time t_{er} is calculated as:

$$t_{er} = t_{et} + \frac{\left\|\overrightarrow{O\,P_1}\right\|}{C}, \tag{14}$$

where C is the speed of light in a vacuum.

3) Collision Analysis: Given our concern about packet collisions at the gateway, it's crucial to identify when packets overlap in time. When considering two packets i and j spanning $[t_{st}(i), t_{et}(i)]$ and $[t_{st}(j), t_{et}(j)]$ respectively, collision at the gateway is determined by the occurrence of any of the following overlap conditions:

1)
$$\begin{aligned} t_{sr}(i) \leq t_{sr}(j) \wedge t_{er}(i) \geq t_{sr}(j) \\ \Rightarrow t_{er}(i) \in [t_{sr}(j), t_{er}(j)] \end{aligned}$$

2)
$$\begin{aligned} t_{sr}(i) \geq t_{sr}(j) \wedge t_{sr}(i) \leq t_{er}(j) \\ \Rightarrow t_{sr}(i) \in [t_{sr}(j), t_{er}(j)] \end{aligned}$$

Fig. 6 illustrates the behavior of the network with four EDs transmitting to a single gateway over time, depicting two pairs of colliding packets with varying degrees of payload interference. Our study classifies any overlap between transmissions on the same gateway and channel as a packet loss event, regardless of the affected packet percentage. This criterion applies to split packets due to the satellite rising above or setting below v_{th} during transmission. However, split, these packets are still considered in collision analysis. Additionally, we do not account for capture effects or Doppler shifts when determining packet validity.

4) Throughput Calculation: The throughput at a given time τ is calculated in terms of successful channel utilization by determining the number of valid (non-collided) packets, denoted as N_{valid}, considered to have reached the gateway within each time analysis interval $\Delta\tau$:

$$\mathcal{S}_{sim}(\tau) = \frac{Nvalid \times ToA}{\Delta\tau}, \tag{15}$$

where $\Delta\tau$ represents the duration of the sampling interval. Since throughput is a measure that lacks significance as an instantaneous value, the selection of $\Delta\tau$ should be guided by the required time granularity in the analysis. As our primary interest lies in determining the mean throughput of the network from an entire scenario, we will compare Eq. 10 with its discrete counterpart in the simulations:

$$\bar{S}_{sim} = \frac{1}{N_s} \sum_{\tau=1}^{N_s} S_L(\tau) \tag{16}$$

where N_s represents the number of sampling intervals.

C. Simulation workflow and analysis

The procedures described throughout this section, illustrated in Fig. 7, are condensed in an algorithm pertaining 8 steps:

1) **Load scenario configurations.**
   Defining parameters of the scenario are configured at the start of the simulation. They are summarized in Table I.
2) **Transmitters deployment**
   Transmitters are randomly positioned within the deployment region, delineated by geographic coordinates: latitude, longitude, and altitude above ground, as outlined in Sections III-A and IV-A, and illustrated in Figure 1.
3) **Calculation of Access Intervals between Transmitters and Satellites.**
   Access times for establishing and losing connectivity between each transmitter and satellite are determined and represented as discrete *events*, as detailed in Section III-A.
4) **Aggregation of Access Intervals.**
   If multiple satellites exist in the scenario and their access regions overlap, access intervals are aggregated to facilitate multi-gateway analysis.
5) **Traffic generation.**
   The methodologies described in Section IV-B1 are executed to generate transmissions for each transmitter-gateway pair within the aggregated intervals.

Parameters
Start and End dates.
Orbital propagator's time step.
Visibility threshold v_{th}.
Packet/transmission duration (ToA)
Duty Cycle percentage, if applicable
Traffic frame generation rate
Number of transmitters to be deployed
Deployment region definition
$\Delta\tau$ analysis interval for the throughput.

TABLE I: List of Parameters for the scenario simulation

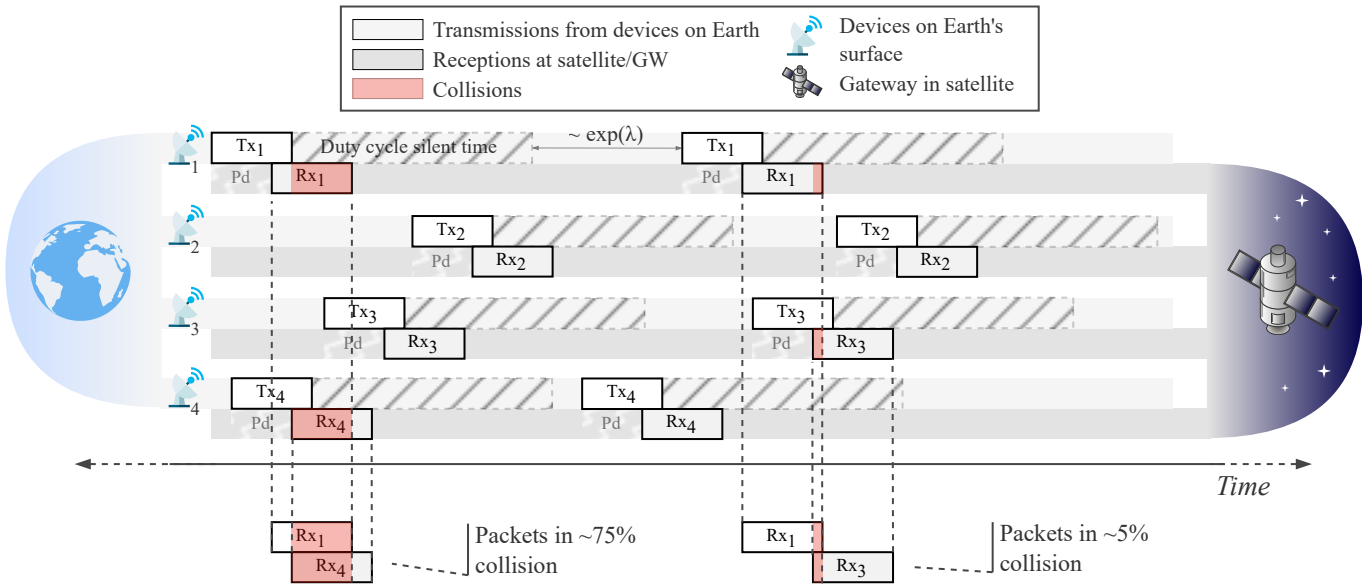

Fig. 6: Illustration of packet collisions in the network, with four EDs transmitting to a single gateway over time. Two pairs of colliding packets are depicted, each with different percentages of payload interference.

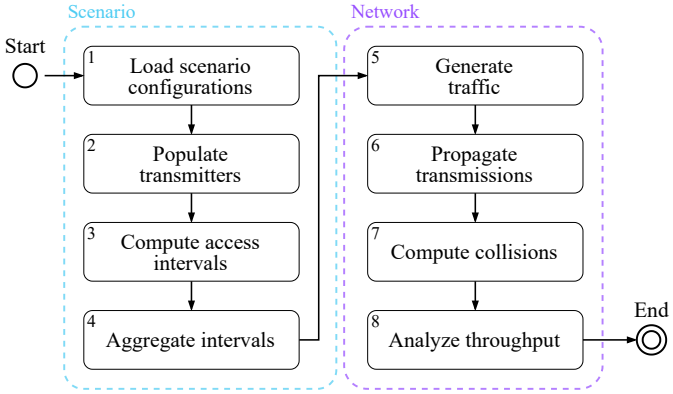

Fig. 7: Simulation workflow depicting the two-fold approach to the simulations: Scenario and Network.

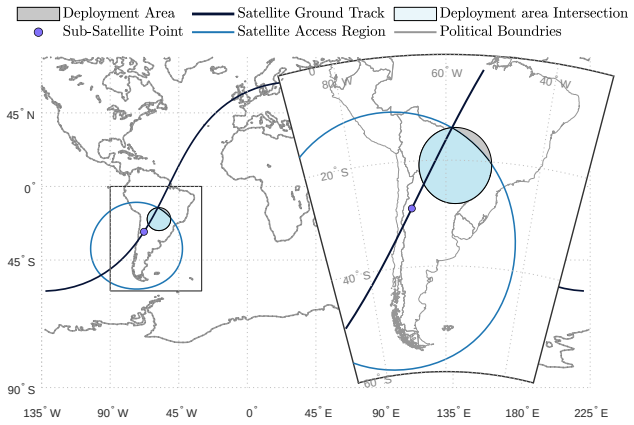

Fig. 8: Snapshot of the single-gateway case study topology after 720 seconds have passed since the simulation started. The Deployment Area is partially covered at $\sim 78\%$.

6) **Propagation of Transmissions.**
   As discussed in Section IV-B2, propagation procedures are initiated only when a transmission or its segment can reach a gateway.
7) **Collision analysis.**
   The techniques elucidated in Section IV-B3 are employed to analyze transmissions at each gateway and identify collision instances. Packets deemed lost are marked as such.
8) **Throughput analysis.**
   Time-dependent interval-based throughput and mean throughput (computed using quadrature) are calculated.

V. Results

We introduce two scenarios as exemplars of single and multi-gateway systems. The first scenario features a transmitter deployment region spanning South America, as depicted in Figs. 1, **??**, and 4. It will be examined as a single-gateway case. This scenario serves two crucial purposes: first, it provides a foundation for fine-tuning simulation parameters, and second, to ease the reader into the multi-gateway case. The second scenario entails a deployment region across Europe designated for multi-gateway analysis. Subsequently, we will manipulate scenario and network parameters to explore how the model adapts simulations across various parameters.

A. Single-gateway case study

In this scenario, we consider a monolithic satellite (single-gateway) setup featuring a single LEO satellite and a circular Ground Device deployment region centered at -21 degrees latitude and -58 degrees longitude, with a radius of 7.1946 degrees ($\sim 800km.$) depicted in Fig. 8. Our analysis focuses on a carefully chosen time interval during which EDs deployed within the network establish and cease contact with

the ascending satellite in its orbit. Additionally, the entire deployment area remains within the visibility range of the gateway throughout a specific interval. Detailed scenario and network configurations can be found in Table III, where the satellite elements' date is set to be the same as the scenario's start date. Network parameters respond to an average inter-arrival time of 0.1 seconds for 500ms Time on Air packets. For reference, using a spreading factor SF10 in the sub-band between 868.0MHz and 868.6MHz, following the EU868 band, a payload length of 40bytes with a preamble length of 8 bytes, explicit header, and CRC, yields a Time on Air of 534.53ms [58], [59].

TABLE II: Scenario and Network configurations for the single-gateway case study

Start date (GMT)			End date (GMT)			step [s]
01-01-2025 16:00:00.000			01-01-2025 16:30:00.000			15
Sat.	a [km]	e	i [deg.]	Ω [deg.]	ω [deg.]	ν [deg.]
1	7371	0	60	295	0	285
$v_{th}[deg.]$	ToA [ms]	DC [%]	λ [$\frac{pack.}{sec.}$]	g [$\frac{pack.}{sec.}$]	$\mathcal{A}(\Omega)[Km^2]$	N° of ch.
20	500	1	5	0.00998	2.0024×10^6	1

Based on these configurations, the deployment area establishes contact with the satellite's access region beginning at 510 seconds into the scenario, and communication is completely lost at 1350 seconds.

We will first examine a subset of results to illustrate the typical behavior of LoRa networks as the number of transmitting devices increases while simultaneously comparing the model's outcomes with simulations. For this purpose, we need to justify the value selected for the sample interval $\Delta\tau$, which is key to obtaining accurate results of the simulations according to Eqs. 15 and 16. An excessively short $\Delta\tau$ implies the potential for only a few or even zero transmissions to be recorded within a given interval, while a $\Delta\tau$ that is too large compromises the resolution of the throughput curve dynamics.

To better grasp these behaviors, numerous simulations encompass various combinations of Time on Air and sample intervals $\Delta\tau$. For each combination, 100 simulations are averaged for 60 nodes. The resulting outcomes are showcased in Figure 9, illustrating the average error between the model's prediction $\bar{S}_L$ and the simulation's quadrature $\bar{S}_{sim}(\tau)$ and the maximum error reached at any time instant t between the model's prediction $S_L(t)$ and the simulation's results $\bar{S}_{sim}(\tau)$, where t lies strictly at $\tau + \frac{\Delta\tau}{2}$. Results evidence a relationship between $\Delta\tau$ and the Time on Air. This behavior must be considered not to undermine the simulation's precision. While increasing $\Delta\tau$ reduces the average error and data dispersion, the behavior for the average error switches at a certain point. Furthermore, distinct values for Time on Air exhibit different values for error and minimal standard deviation. With this in mind, given that we have $ToA = 500ms.$, a $\Delta\tau = 15s.$ is selected to yield average errors less than 3% and a std. deviation less than 0.013.

First, we will show the average results of 500 simulations for scenarios involving 10, 50, and 90 EDs, as depicted in Figure 10. For the cases with 10 and 50 EDs, we observe that throughput rises as access to the deployment region (and consequently the number of devices within reach) increases.

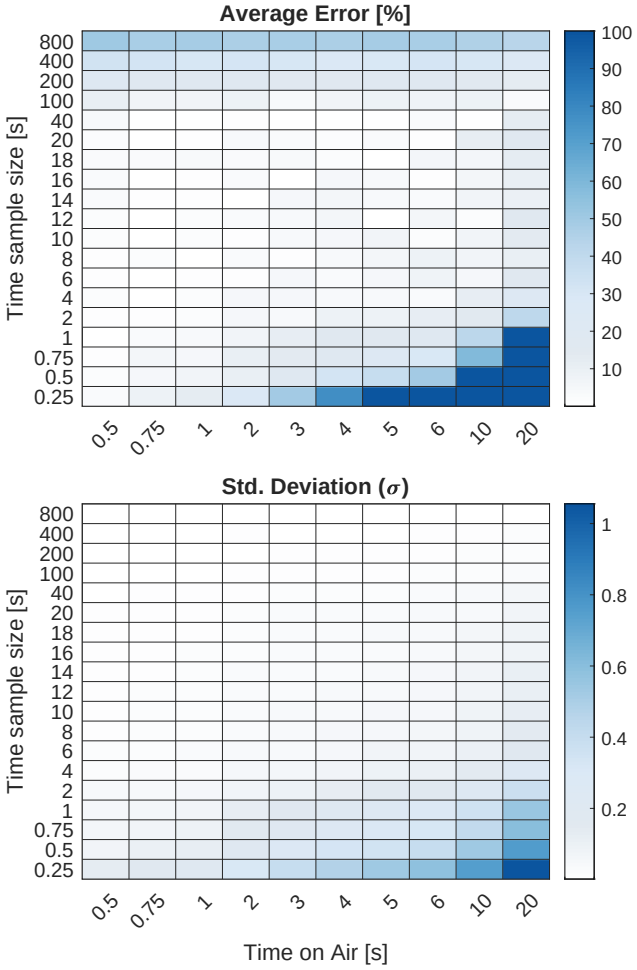

Fig. 9: Comparison of Model Predictions and Simulation Results: Heatmap depicting the average error and standard deviation for various combinations of Time on Air and sample intervals $\Delta\tau$.

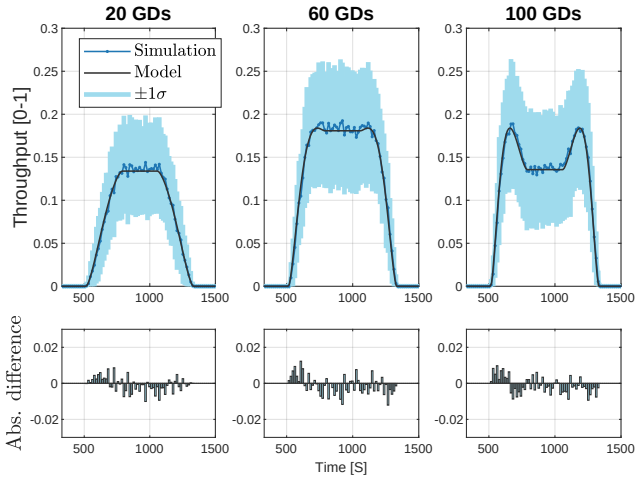

Fig. 10: Comparison of Model and Simulation results for throughput dynamics, depicting absolute differences among them, with increasing EDs: 10, 50, and 90 Cases.

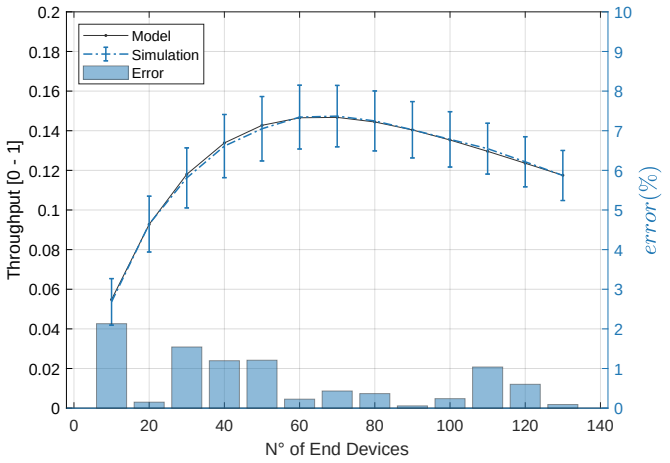

Fig. 11: Comparison of average throughput between simulation and model results. Note that while the absolute difference between results increases with the number of EDs, as evidenced by the small gap between curves, the percentage difference consistently remains below 3%.

Throughput reaches a peak before beginning to decline as access diminishes; this is noticeable in the case of 90 EDs, where a dip in throughput is seen. This dip is attributed to the increasing number of collisions overwhelming the network, thereby reducing throughput during maximum access intervals. It is also noticeable that the difference $S_L(t) - \bar{S}_{sim}(\tau)$ seems to increase when rapid changes (i.e., gradient or slope) occur in the predicted throughput curve. To study how the average throughput behaves as a function of the number of devices, simulations are performed for a 10 to 130 EDs range in steps of 10, and the difference with the model's prediction is now expressed as a percentage $error(\%)$.

The results in Fig. 11 illustrate the average throughput curve for both the model and the simulations. They demonstrate the accuracy of the model's predictions and an anticipated pattern: throughput increases proportionally with the number of devices until network collisions occur, resulting in frame loss.

We also want to explore a potential correlation between the satellite's altitude and the model's accuracy. The lower the orbit's altitude over the Earth's surface, the transmissions will experience propagation delay but need to reach a faster satellite. A higher satellite means that transmissions need more time to reach the gateway, but its relative speed diminishes. Simulations are performed for altitudes within the LEO spectrum for the same EDs range. The average results for 200 simulations on each ED/altitude pair are shown as two heat maps in Fig. 12. The error between the model's prediction and the simulations for the overall scenario throughput falls consistently under 6%, and the std. deviation, under 2%. Albeit small, results suggest a correlation between altitude and accuracy. Specifically, decreasing the orbit's altitude slightly reduces the accuracy of the model's predictions. This becomes more apparent when the average errors and standard deviations are each averaged across the number of EDs and presented as

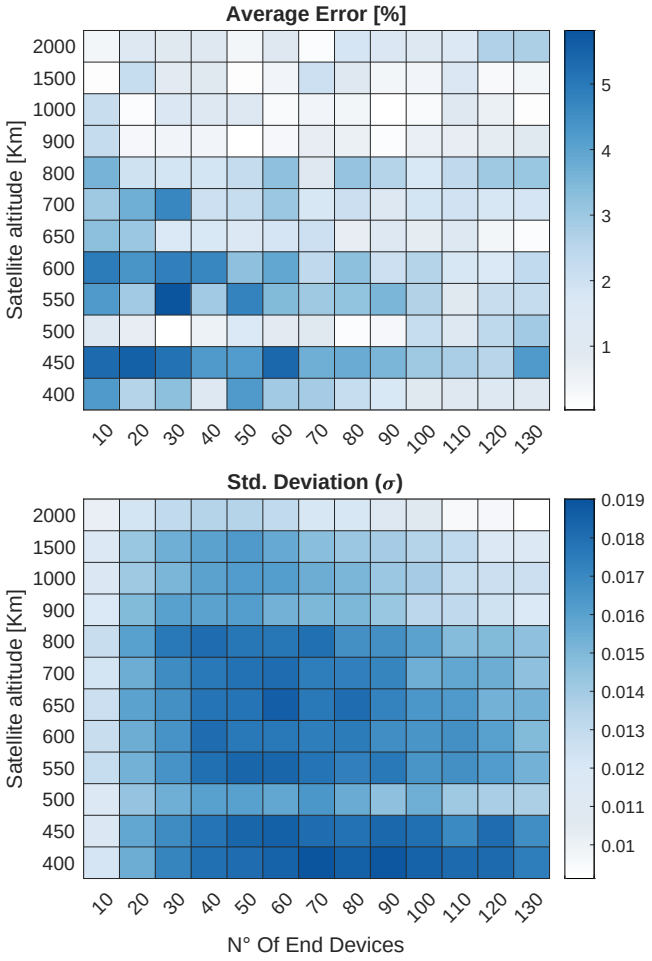

Fig. 12: Average error and standard deviation across distinct number of EDs and satellite altitudes for the single-gateway scenario.

a function of satellite altitude. This is illustrated in Fig. 13.

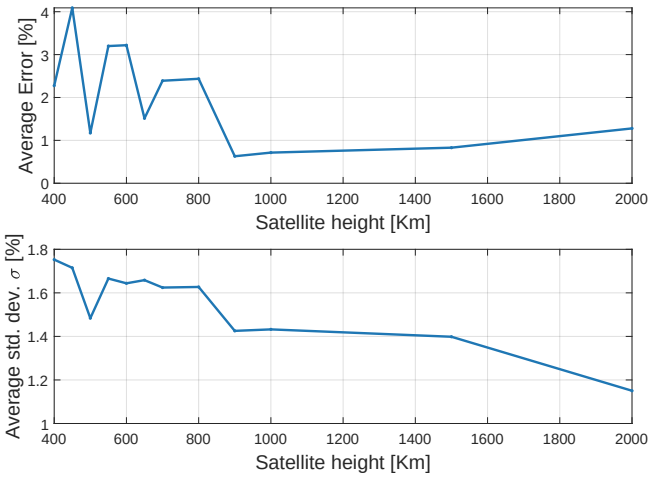

Fig. 13: Average error and standard deviation averaged across distinct EDs, as a function of satellite height.

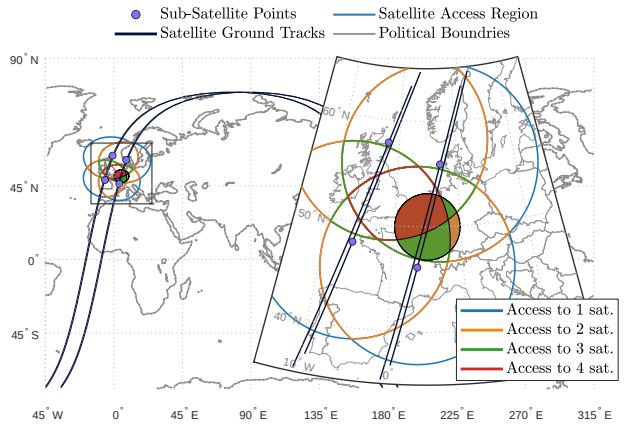

Fig. 14: Snapshot of the multi-gateway case study topology after 840 seconds have passed since the simulation started. The Deployment Area is completely covered by at least 2 satellites and partially covered by 3 or 4 satellites.

TABLE III: Scenario and Network configurations for the multi-gateway case study

Start date (GMT)			End date (GMT)			step [s]
01-01-2025 16:00:00.000			01-01-2025 16:30:00.000			15
Sat.	a [km]	e	i [deg.]	Ω [deg.]	ω [deg.]	ν [deg.]
1	6871	0	98	160	0	70
2	6871	0	98	160	0	80
3	6871	0	98	150	0	78
4	6871	0	98	150	0	68
$v_{th}[deg.]$	ToA [ms]	DC [%]	λ [$\frac{pack.}{sec.}$]	g [$\frac{pack.}{sec.}$]	$\mathcal{A}(\Omega)[Km^2]$	$N°$ of ch.
20	500	1	5	0.00998	3.8515×10^5	1

B. Multi-gateway deployment

In this scenario, we consider a constellation setup featuring four LEO satellites and a circular Ground Device deployment region centered at 50 degrees latitude and 5 degrees longitude, with a radius of 3.1442 degrees ($\sim 350km.$) depicted in Fig. 14. The satellites fly on two orbital planes in retrograde motion at 98 degrees of inclination. For the chosen scenario time span, various satellites are visible at different instants of time from any given point in the ED deployment area.

We assume that the error in multi-gateway, in terms of collective sensibility to sample step size $\Delta\tau$, follows the same behavior as for individual satellites, so a $\Delta\tau = 15s.$ is chosen for the simulations. Detailed scenario and network configurations can be found in Table III, where the satellite elements' date is set to be the same as the scenario's start date. Network parameters respond to an average inter-arrival time of 0.1 seconds for 500ms ToA packets. The dynamics of constellation access to the Deployment Region are more complex than the single-gateway case. This complexity arises from the fact that access regions, in addition to moving independently, overlap across the deployment region, as anticipated in Sec. III-A. Fig. 15 illustrates both the access from the deployment region to *at least k* satellites and access from each satellite. As in the single-gateway case study, 200 simulations are averaged for each case (10 to 130 EDs range in steps of 10), and the difference with the model's prediction is expressed as a percentage $error(\%)$. A similar comparison to that in Fig. 10 is illustrated in 16. In this case, it is also hinted that the difference $S_L(t) - \bar{S}_{sim}(\tau)$ seems to increase when changes occur in the predicted throughput curve, and these differences are greater than the single-gateway case. Average results are depicted in Fig. 17. As with the single-gateway case, we will manipulate network and scenario parameters to explore the model's accuracy under different configurations. First, we will vary the transmissions' ToA from 250 ms to 8 seconds. Both average error and standard deviation are illustrated as heatmaps in Fig. 18. Results evidence a correlation between ToA and average error, consistent with 9. Finally, we will adjust the constellation's altitude, a change that, in contrast to the single-gateway case, carries significant implications beyond altering relative speeds and range between End Devices and satellites. Specifically, changing the semi-major axis of each satellite implies varying the relative distances between them, thereby altering the dynamic intersecting behavior of access regions. Results are illustrated as heatmaps in Fig. 19. We don't find a significant correlation in average error between a number of devices and different altitudes, but we do notice it jumps up to 3.3 % across different heights. However, this pattern differs for the standard deviation, which exhibits a clear local maximum between 50 and 70 devices, and altitudes ranging from 800 to 1500 km.

VI. Conclusions

This paper introduces an analytical approach to assess network throughput in multi-gateway satellite IoT missions, incorporating static network models with advanced astrodynamics tools and simulations that address the complexities of constellation-based deployments.

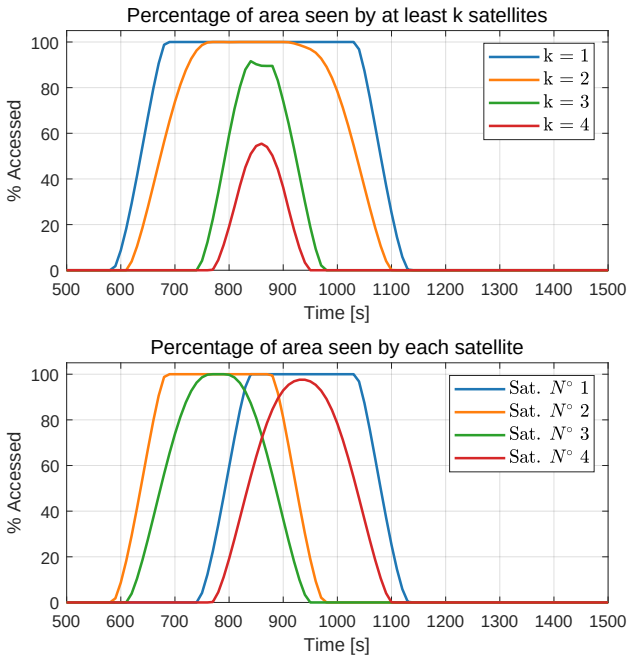

Fig. 15: Percentage of access to the deployment region by *at least k* satellites (top) and by each satellite (bottom).

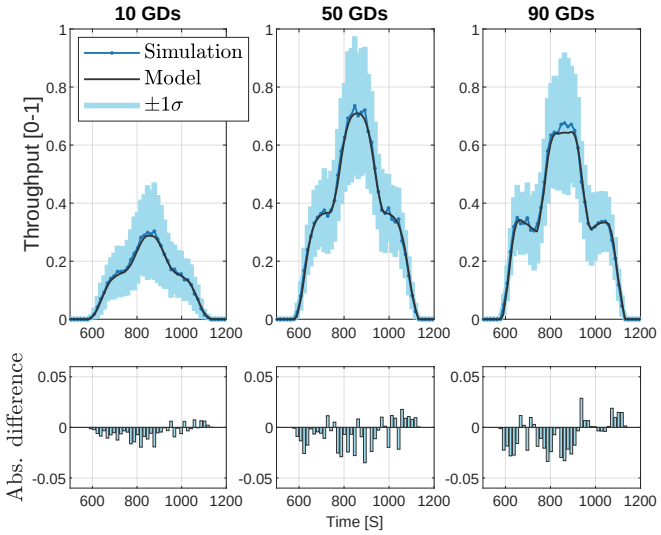

Fig. 16: Comparison of Model and Simulation results for throughput dynamics, with increasing EDs: 10, 50, and 90 Cases. Absolute differences are plotted below.

In addition to the overarching rapid analysis of LoRaWAN-based DtS-IoT constellations, this study delves into specific scenarios to analyze single and multi-gateway systems. With deployment regions within South America and Europe, these scenarios are benchmarks for assessing network performance and adaptability across varying parameters. Results from simulations highlight several interesting outcomes:

- There is an intricate relationship between time sampling time and Time on Air, underscoring the importance of considering these factors for maintaining simulation precision. Parameter adjustments reveal distinct error and standard deviation trends, shedding light on optimal simulation configurations for minimizing data dispersion and ensuring accurate throughput predictions in LEO constellations.
- Observations from cases with different numbers of EDs elucidate the impact of access to deployment regions on throughput. While throughput initially increases with greater access, reaching a peak before declining due to increased network collisions, simulations demonstrate the model's ability to predict these trends with remarkable accuracy.
- Investigating the relationship between satellite altitude and model accuracy reveals intricate dynamics shaped by orbit altitude, resulting in differences up to 6% for the single-gateway scenario and 4% for the multi-gateway scenario. Given the minimal changes in orbital altitude —where variations in distance less than 2000 km translate to delay increments of less than 7 ms— in LEO, we conclude that orbital speed significantly influences model accuracy, and further studies are needed to adapt the model to maintain its precision.

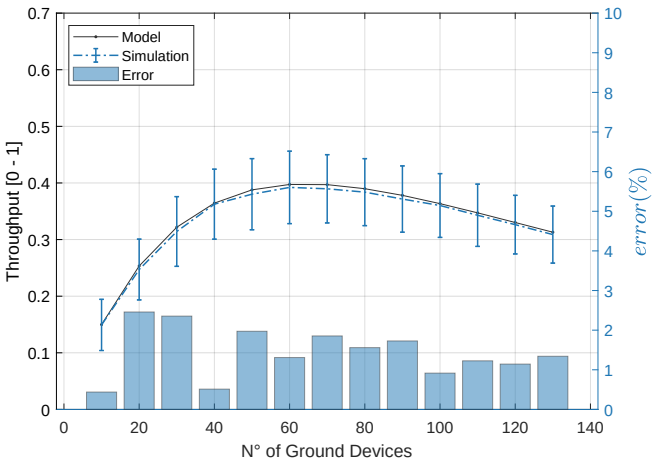

Fig. 17: Comparison of average throughput between simulation and model results. Note that while the absolute difference between results increases with the number of EDs, as evidenced by the small gap between curves, the percentage difference consistently ranges under 3%, as shown in the bar plot.

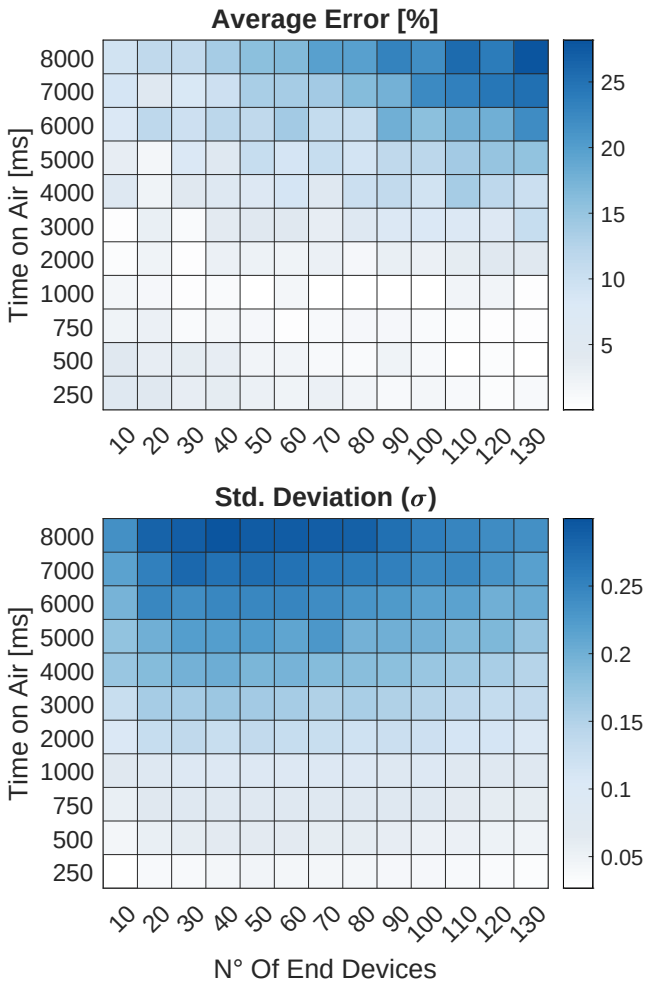

Fig. 18: Average error and standard deviation across distinct number of EDs and transmissions ToA for the multi-gateway scenario.

- Our analysis reveals heightened complexity in constellation access dynamics stemming from overlapping access regions and independent movement patterns. This behavior is hinted at in the model's accuracy when predicting rapid changes in throughput, a phenomenon that becomes more noticeable in the multi-gateway scenario. Despite this complexity, simulations consistently align closely with model predictions, with average percentage differences in throughput remaining under 4% across varying EDs.

This study enhances our understanding of LoRaWAN-based DtS-IoT constellations, offering insights into network performance, adaptability, and the impact of satellite parameters. Correlations between throughput and various parameters underscore optimization challenges. Designing and operating such constellations, especially through simulations, present significant challenges, which can be addressed with fast and accurate analytical models, aiding decisions crucial for maximizing satellite-based IoT connectivity.

Future work will target *structured access methods* like NB-IoT and *frequency-hopping* techniques like LR-FHSS and Mioty [60]. Moreover, the author's roadmap includes evaluating the analysis and simulation against more realistic emulation test beds [61].

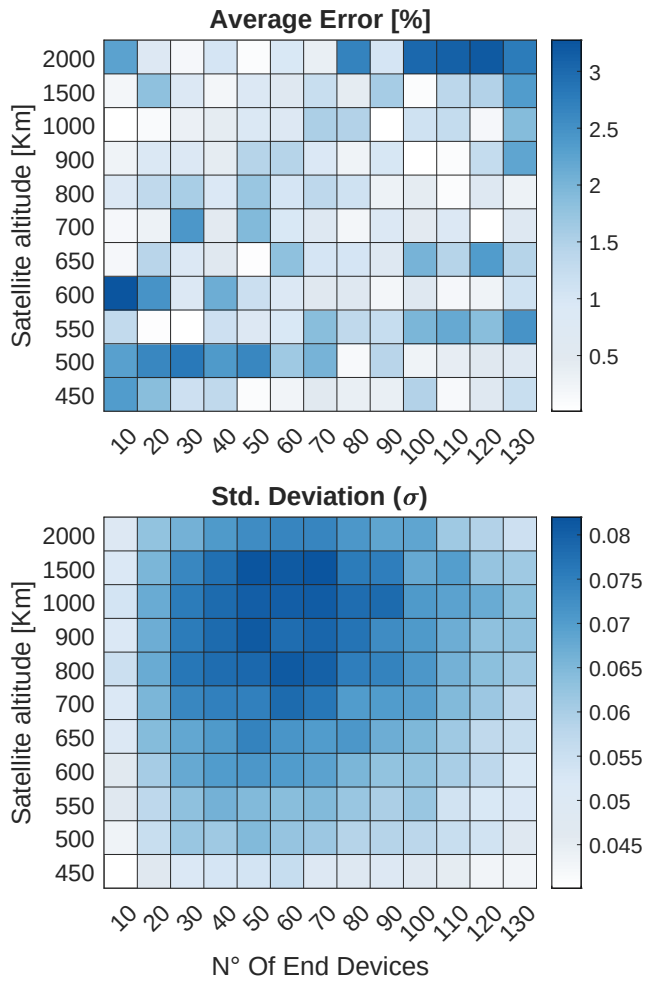

Fig. 19: Average error and standard deviation across distinct number of EDs and constellation altitudes for the multi-gateway scenario.

Acknowledgement

This research has received support from Project STICAMSUD 21-STIC-12, the European Union's Horizon 2020 R&D program under the Marie Skłodowska-Curie grant agreement No 101008233 (MISSION project), and the French National Research Agency (ANR) under the project ANR-22-CE25-0014-01.

References

[1] M. R. Palattella, N. Accettura, X. Vilajosana, T. Watteyne, L. A. Grieco, G. Boggia, and M. Dohler, "Standardized Protocol Stack for the Internet of (Important) Things," *IEEE Communications Surveys Tutorials*, vol. 15, no. 3, pp. 1389–1406, Third 2013.

[2] R. S. Sinha, Y. Wei, and S.-H. Hwang, "A Survey on LPWA Technology: LoRa and NB-IoT," *ICT Express*, vol. 3, no. 1, pp. 14 – 21, 2017.

[3] N. Zhang, M. Wang, and N. Wang, "Precision Agriculture—a Worldwide Overview," *Computers and Electronics in Agriculture*, vol. 36, no. 2, pp. 113 – 132, 2002.

[4] M. De Sanctis, E. Cianca, G. Araniti, I. Bisio, and R. Prasad, "Satellite Communications Supporting Internet of Remote Things," *IEEE Internet of Things Journal*, vol. 3, no. 1, pp. 113–123, Feb 2016.

[5] D. Minoli, *Building the Internet of Things with IPv6 and MIPv6: The Evolving World of M2M Communications*, 1st ed. Wiley Pub., 2013.

[6] J. Wertz, *Orbit Constellation Design and Management*, 1st ed., ser. Space Technology Library. Dordrecht: Springer Dordrecht, 2001.

[7] M. R. Palattella and N. Accettura, "Enabling Internet of Everything Everywhere: LPWAN with Satellite Backhaul," in *2018 Global Info. Infra. and Networking Symposium (GIIS)*. IEEE, oct 2018, pp. 1–5.

[8] I. Bisio and M. Marchese, "Efficient Satellite-Based Sensor Networks for Information Retrieval," *IEEE Syst. J.*, vol. 2, pp. 464–475, Dec. 2008.

[9] J. A. Fraire, S. Céspedes, and N. Accettura, "Direct-To-Satellite IoT - A Survey of the State of the Art and Future Research Perspectives," in *ADHOC-NOW 2019: Ad-Hoc, Mobile, and Wireless Networks*, Luxembourg, Luxembourg, Oct. 2019, pp. 241–258.

[10] Y. Kawamoto, H. Nishiyama, Z. M. Fadlullah, and N. Kato, "Effective Data Collection Via Satellite-Routed Sensor System (SRSS) to Realize Global-Scaled Internet of Things," *IEEE Sensors Journal*, vol. 13, no. 10, pp. 3645–3654, Oct 2013.

[11] T. Ferrer, S. Céspedes, and A. Becerra, "Review and Evaluation of MAC Protocols for Satellite IoT Systems Using Nanosatellites," *Sensors*, vol. 19, no. 8, p. 1947, apr 2019.

[12] LoRa Alliance Technical Committee, "LoRaWAN 1.1 specification," LoRa Alliance, Tech. Rep., 2017.

[13] Semtech, "Loratm modulation basics," 2015.

[14] J. Petajajarvi, K. Mikhaylov, A. Roivainen, T. Hanninen, and M. Pettissalo, "On the coverage of lpwans: range evaluation and channel attenuation model for lora technology," in *2015 14th International Conference on ITS Telecommunications (ITST)*, 2015, pp. 55–59.

[15] M. Ballerini, T. Polonelli, D. Brunelli, M. Magno, and L. Benini, "Nb-iot versus lorawan: An experimental evaluation for industrial applications," *IEEE Transactions on Industrial Informatics*, vol. 16, no. 12, pp. 7802–7811, 2020.

[16] The Things Network, *Duty Cycle*. [Online]. Available: https://www.thethingsnetwork.org/docs/lorawan/duty-cycle/

[17] N. Accettura and B. Prabhu, "Ubiquitous multi-gateway LoRa networks: models and performance evaluation," Aug. 2020, working paper or preprint. [Online]. Available: https://hal.laas.fr/hal-02914373

[18] Z. Zhou, N. Accettura, R. Prévost, and P. Berthou, "Lightweight synchronization to nb-iot enabled leo satellites through doppler prediction," in *2023 19th International Conference on Wireless and Mobile Computing, Networking and Communications (WiMob)*, 2023, pp. 218–223.

[19] A. Talgat, M. A. Kishk, and M. S. Alouini, "Stochastic geometry-based analysis of leo satellite communication systems," *IEEE Communications Letters*, vol. 25, no. 8, pp. 2458–2462, 2021.

[20] H. Chen, H. Wu, Z.-L. Li, and J. Tu, "An improved computational geometry method for obtaining accurate remotely sensed products via convex hulls with dynamic weights: A case study with leaf area index," *IEEE Journal of Selected Topics in Applied Earth Observations and Remote Sensing*, vol. 12, no. 7, pp. 2308–2319, 2019.

[21] S. M. Henn, J. A. Fraire, and H. Hermanns, "Polygon-based algorithms for n-satellite constellations coverage computing," *IEEE Transactions on Aerospace and Electronic Systems*, vol. 59, no. 5, pp. 7166–7182, 2023.

[22] Z. Song, X. Hu, M. Wang, and G. Dai, "Judgement theorems and an approach for solving the constellation-to-ground coverage problem," *Mathematical Problems in Engineering*, vol. 2018, pp. 1–10, 02 2018.

[23] Argos System CLS, *ARGOS*. [Online]. Available: https://www.argos-system.org/

[24] A. Carlotto and J. Juárez, "Estudio sobre la localización de plataformas del sistema dcs del satélite sac-d," in *2014 IEEE Biennial Congress of Argentina (ARGENCON)*, 2014, pp. 722–726.

[25] R. Patmasari, I. Wijayanto, R. Deanto, Y. Gautama, and H. Vidyaningtyas, "Design and realization of automatic packet reporting system (APRS) for sending telemetry data in nano satellite communication system," *Journal of Measurements, Electronics, Communications, and Systems*, vol. 4, no. 1, pp. 1–7, 2018.

[26] L. Vangelista, "Frequency Shift Chirp Modulation: The LoRa modulation," *IEEE Signal Proc. Letters*, vol. 24, no. 12, pp. 1818–1821, 2017.

[27] N. Accettura, E. Alata, P. Berthou, D. Dragomirescu, and T. Monteil, "Addressing Scalable, Optimal, and Secure Communications over LoRa networks: Challenges and Research Directions," *Internet Technology Letters*, vol. 1, no. 4, p. e54, jul 2018.

[28] I. T. Union, "Annex 16 to working party 4a chairman's report - working document on developing an itu-r small satellite handbook," International Telecommunication Union, Tech. Rep., 2021.

[29] The Things Network Global Team, *LoRa World Record Broken: 832km using 25mW*, 2020 (accessed May 29, 2020). [Online]. Available: https://www.thethingsnetwork.org/article/lorawan-world-record-broken-twice-in-single-experiment-1

[30] S. Demetri, M. Zúñiga, G. P. Picco, F. Kuipers, L. Bruzzone, and T. Telkamp, "Automated Estimation of Link Quality for LoRa: A Remote Sensing Approach," in *Proceedings of the 18th International Conference on Information Processing in Sensor Networks*. Montreal: ACM, 2019, pp. 145–156.

[31] Y. Qian, L. Ma, and X. Liang, "The Acquisition Method of Symmetry Chirp Signal Used in LEO Satellite Internet of Things," *IEEE Communications Letters*, vol. 23, no. 9, pp. 1572–1575, 2019.

[32] A. Doroshkin, A. Zadorozhny, O. Kus, and V. Prokopyev, "Experimental Study of LoRa Modulation Immunity to Doppler Effect in CubeSat Radio Communications," *IEEE Access*, vol. PP, no. c, p. 1, 2019.

[33] G. Colavolpe, T. Foggi, M. Ricciulli, Y. Zanettini, and J. Mediano-Alameda, "Reception of LoRa Signals From LEO Satellites," *IEEE TAES*, vol. 55, no. 6, pp. 3587–3602, 2019.

[34] LoRa Alliance Tech. Committee, *LoRaWAN™ 1.1 Spec.*, Oct. 2017, v1.1.

[35] A. Lavric and V. Popa, "Internet of Things and LoRa Low-Power Wide-Area Networks: a Survey," in *2017 International Symposium on Signals, Circuits and Systems (ISSCS)*. IEEE, 2017, pp. 1–5.

[36] T. Polonelli, D. Brunelli, and L. Benini, "Slotted aloha overlay on lorawan - a distributed synchronization approach," in *2018 IEEE 16th International Conference on Embedded and Ubiquitous Computing (EUC)*, 2018, pp. 129–132.

[37] D. Bankov, E. Khorov, and A. Lyakhov, "Mathematical model of lorawan channel access," in *2017 IEEE 18th International Symposium on A World of Wireless, Mobile and Multimedia Networks (WoWMoM)*, 2017, pp. 1–3.

[38] ——, "Mathematical model of lorawan channel access with capture effect," in *2017 IEEE 28th Annual International Symposium on Personal, Indoor, and Mobile Radio Communications (PIMRC)*, 2017, pp. 1–5.

[39] B. Paul, "A novel mathematical model to evaluate the impact of packet retransmissions in lorawan," *IEEE Sensors Letters*, vol. 4, no. 5, pp. 1–4, 2020.

[40] B. Błaszczyszyn and P. Muhlethaler, "Analyzing lora long-range, low-power, wide-area networks using stochastic geometry," 03 2019, pp. 119–126.

[41] N. Aftab, S. A. R. Zaidi, and D. McLernon, "Scalability analysis of multiple lora gateways using stochastic geometry," *Internet of Things*, vol. 9, p. 100132, 2020. [Online]. Available: https://www.sciencedirect.com/science/article/pii/S2542660519301027

[42] J. A. Fraire, P. Madoery, A. Mehdi, O. Iova, and F. Valois, "Simulating LoRa-Based Direct-to-Satellite IoT Networks with FLoRaSat," in *WoWMoM 2022 - IEEE 23rd International Symposium on a World of Wireless, Mobile and Multimedia Networks*, Belfast, United Kingdom, Jun. 2022. [Online]. Available: https://hal.science/hal-03698223

[43] L. Chasserat, N. Accettura, and P. Berthou, "Lorasync: energy efficient synchronization for scalable lorawan," *Transactions on emerging telecommunications technologies*, vol. 35, no. 2, Feb. 2024. [Online]. Available: https://laas.hal.science/hal-03694383

[44] F. A. Tondo, M. Afhamisis, S. Montejo-Sánchez, O. L. A. López, M. R. Palattella, and R. D. Souza, "Multiple channel lora-to-leo scheduling for direct-to-satellite iot," *IEEE Access*, vol. 12, pp. 30 627–30 637, 2024.

[45] D. A. Vallado and W. D. McClain, *Fundamentals of astrodynamics and applications*, 4th ed. Hawthorne, California: Microcosm Press, 2013, vol. The space technology library.

[46] D. Vallado, P. Crawford, R. Hujsak, and T. Kelso, *Revisiting Spacetrack Report #3*. AIAA, 2006. [Online]. Available: https://arc.aiaa.org/doi/abs/10.2514/6.2006-6753

[47] L. Maisonobe, V. Pommier, and P. Parraud, "Orekit: An open source library for operational flight dynamics applications," in *4th International Conference on Astrodynamics Tools and Techniques*, 2010, pp. 3–6.

[48] F. Martínez, C. Ogayar, J. R. Jiménez, and A. J. Rueda, "A simple algorithm for boolean operations on polygons," *Advances in Engineering Software*, vol. 64, pp. 11–19, 2013.

[49] F. P. Preparata and M. I. Shamos, *Computational Geometry: An Introduction*, 1st ed. Springer New York, NY, 01 2008.

[50] M. Nugnes, C. Colombo, and M. Tipaldi, "Coverage area determination for conical fields of view considering an oblate earth," *Journal of Guidance, Control, and Dynamics*, vol. 42, no. 10, pp. 2233–2245, oct 2019. [Online]. Available: https://doi.org/10.2514%2F1.g004156

[51] "Compass project," accessed: 2022-09-01. [Online]. Available: https://www.compass.polimi.it/

[52] D. R. Luders, "Satellite networks for continuous zonal coverage," *ARS Journal*, vol. 31, no. 2, pp. 179–184, 1961. [Online]. Available: https://doi.org/10.2514/8.5422

[53] Y. Seyedi and S. M. Safavi, "On the analysis of random coverage time in mobile leo satellite communications," *IEEE Communications Letters*, vol. 16, no. 5, pp. 612–615, 2012.

[54] G. V. Mozhaev, "Capabilities of kinematically regular satellite systems with symmetry groups of the second type in the problem of continuous single coverage of the earth," *Cosmic Research*, vol. 43, no. 3, pp. 205–212, May 2005.

[55] P. Sengupta, S. Vadali, and K. Alfriend, "Satellite orbit design and maintenance for terrestrial coverage," *Journal of Spacecraft and Rockets*, vol. 47, pp. 177–187, 01 2010.

[56] Y. Zhang, S. Bai, and C. Han, "Geometric analysis of a constellation with a ground target," *Acta Astronautica*, vol. 191, 11 2021.

[57] Z. Song, H. Liu, D. Guangming, W. Maocai, and C. Xiaoyu, "Cell area-based method for analyzing the coverage capacity of satellite constellations," *International Journal of Aerospace Engineering*, vol. 2021, no. 20, p. 10, 2021.

[58] Lorawan regional parameters. The Things Network. Accessed on April 27, 2024. [Online]. Available: https://www.thethingsnetwork.org/docs/lorawan/regional-parameters/eu868/

[59] N. Accettura, S. Medjiah, B. Prabhu, and T. Monteil, "Low power radiolocation through long range wide area networks: A performance study," in *2017 IEEE 13th International Conference on Wireless and Mobile Computing, Networking and Communications (WiMob)*, 2017, pp. 1–8.

[60] N. D. Sunkara, "MIoTy Overview: a Mathematical Description of the Physical Layer," Thesis and Dissertation, ADUA, 2022. [Online]. Available: https://hdl.handle.net/20.500.12608/30735

[61] M. Afhamisis, S. Barillaro, and M. R. Palattella, "A testbed for lorawan satellite backhaul: Design principles and validation," in *2022 IEEE International Conference on Communications Workshops (ICC Workshops)*, 2022, pp. 1171–1176.